International Journal of Nanoelectronics and Materials
IJNeaM
ISSN 1985-5761 | E-ISSN 2232-1535

Effect of post-annealing temperature on structural, morphological, optical, and electrical properties of Sb-doped SnO_2 thin films for optoelectronic applications

Subramanyam Darla [a,b*], Chandrasekhara Reddy Kuntalo [a,c], Rajesh Kumar Borra [d]

[a] *Research and Development Centre, Bharathiar University, Coimbatore - 641046, Tamil Nadu, India*
[b] *Department of Physics, STSN Govt Degree College, Kadiri - 515591, Andhra Pradesh, India*
[c] *Department of Physics, Govt. Degree College, Uravakonda- 515812, Anantapur, Andhra Pradesh, India*
[d] *Department of Physics, GITAM (Deemed to be University), Visakhapatnam-530045, Andhra Pradesh, India*
** Corresponding author. Tel.: +91-9493246090; e-mail: subramanyamdarla@gmail.com*

Received 21 March 2025, Revised 23 May 2025, Accepted 3 July 2025

ABSTRACT

Antimony(Sb)-doped tin oxide (SnO_2) thin films were grown by sol-gel spin coating and post-annealed from 150 to 350 °C. XRD, FESEM, AFM, XPS, UV-VIS-NIR spectroscopy, and four-point probe technique were used to study the physical properties of Sb-doped SnO_2 (ATO) films. XRD studies of Sb-doped SnO_2 films exhibit a tetragonal rutile structure. The crystallite size of ATO films increased from 19 to 45 nm with post-annealing temperature. The morphology of ATO films shows a dense structure with a homogeneous grain distribution. The optical bandwidth of Sb-doped SnO_2 films decreased from 3.36 to 3.08 eV due to reduced defect densities and grain boundaries. The electrical resistance of Sb-doped SnO_2 films reduces from 2.64×10^{-3} to 1.74×10^{-3} Ω.cm due to improved crystallinity and decreased interstitial atoms with increased post-annealing temperature.

Keywords: *Thin films, Sol-gel, Sb-doped SnO_2, X-ray diffraction, Optical parameters, Electrical resistivity*

1. INTRODUCTION

Tin oxide (SnO_2) is a transparent conducting oxide (TCO) material with high optical transmittance, electrical conductivity in the visible region, high reflectivity at the near-infrared region, and a wide band gap (~3.6 eV). These materials had potential applications in optoelectronics, e.g., transparent electrodes, solar cells, field effect transistors, window materials for solar cells, gas sensors, etc., [1-3]. SnO_2 exhibits higher thermal resistance than indium-doped tin oxide, so the films have good abrasion scratch resistance [4, 5]. Extrinsic or intrinsic dopants can alter the band gap of SnO_2. Antimony (Sb) is an extrinsic doping material for SnO_2 that gains versatility because of its cost-effectiveness and non-toxic properties compared to other dopants, such as fluorine and indium [6, 7]. The n-type doping in which a valence state Sb^{5+} increases the conductivity of SnO_2 because these ions occupy substitutional cations within the Sn^{4+} site, increasing the electron density. The presence of Sb^{5+} donor ions shifts the Fermi level (E_f) close to the conduction band [8]. The ionic radii of Sb^{5+}~0.74 Å are close to Sn^{4+}~0.83 Å, producing the lattice distortion from substitutional Sb^{5+} donors [9]. Sb-doped SnO_2 (ATO) is an attractive material for gas sensor applications because the surface sensitivity of this material makes it a selective material [10-12]. The annealing treatment can enhance the performance of gas sensors and optoelectronic applications, leading to changes in the microstructural factors such as film density, pore size, and adsorption sites [13, 14].

Different deposition methods, such as sputtering [15], pulsed laser deposition (PLD) [16], spray pyrolysis [17], and sol-gel [18], have been used to prepare Sb-doped SnO_2 films. Among these, the sol-gel spin coating can be preferable because of good homogeneity, large area coatings, and low processing temperature. The present paper will focus on the annealing effect on the physical properties of Sb-doped SnO_2 films.

2. EXPERIMENTAL

Sb-doped SnO_2 (ATO) films were prepared with the chemicals of high purity (AR grade, Sigma-Aldrich) using tin (II) chloride dihydrate ($SnCl_2.2H_2O$) as a precursor, Antimony (III) chloride ($SbCl_3$) as a dopant, 2-methoxy ethanol as a solvent, and monoethanolamine (MEA) as a stabilizer. First, 0.2M of $SnCl_2.2H_2O$ and 0.05 M of $SbCl_3$ had to be dissolved within 50 ml of distilled water individually, and then both solutions were stirred for two hours at 350 rpm at 80 °C. The MEA is used as a stabilizer and added at a 5 ml/minute drop rate to achieve a homogeneous and transparent solution. The final solution was aged for over 48 hours to produce a sol-gel. The final gel solution had been spin-coated upon the glass substrates at a rotational speed of 2500 rpm to form ATO films and post-annealed from 150 to 300 °C. The measured film thickness from the spectroscopic ellipsometer (J.A. Woollam, Alpha-SE) is 165-280 nm. The crystallinity of Sb-doped SnO_2 films was studied with an X-ray diffractometer (Bruker D8) with CuK_α radiation (λ=0.154nm). The morphological analysis of Sb-doped SnO_2 films was employed with FESEM and AFM

(Ultra 55, Karl Zeiss & Bruker Icon). XPS (Axis Ultra-165) analyzes the elemental composition of ATO films. The optical absorption of ATO films was employed using a UV-Vis-NIR (Hitachi U-2900) spectrophotometer. The electrical resistivity of ATO films was measured with the four-point probe method using a Keithley 2450 source meter instrument.

3. RESULTS AND DISCUSSION

3.1. Structural studies

XRD spectra of Sb-doped SnO_2 (ATO) films post-annealed from 150 to 350 °C are shown in Figure 1. The XRD spectra show intense diffraction peaks with orientation along (1 1 0), (1 0 1), and (2 1 1). The ATO films exhibit rutile tetragonal structure of SnO_2 compared with XRD peak positions corresponding to those on JCPDS Card #41-1445. The diffraction peaks become sharper and more crystalline with increased annealing treatment from 150 to 350 °C. The lattice constants a, c, and volume of ATO films were calculated using the formulas reported by Ramarajan et al. [19]. The lattice constant values increase with post-annealing temperature, weakening the interatomic bonding strength, generating more stacked carriers, and decreasing the band gap between the shells of conduction and valence.

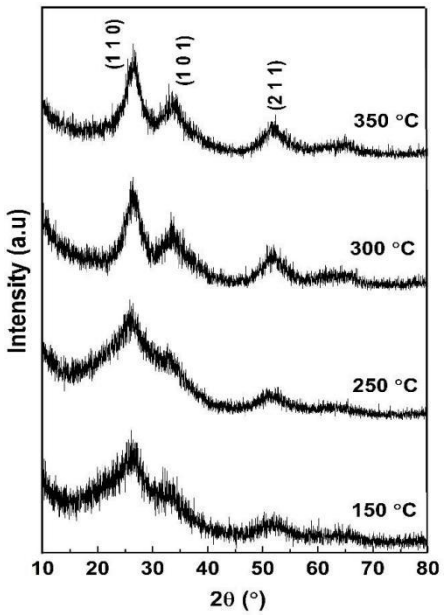

Figure 1. XRD patterns of ATO films

ATO film's crystallite size (D) has been determined using the Debye–Scherrer equation [20]. The thermal annealing treatment increased the average crystallite size from 19 to 45 nm. As the thermal annealing rises from 150 to 350 °C, the FWHM of XRD peaks decreases, resulting in an increase in crystallite size and a decrease in dislocation density from 2.77×10^{15} to 0.45×10^{15} nm^{-2}. The ATO film's micro-strain was evaluated by the formula $\varepsilon = \beta/\tan\theta$. It is noticed that the micro-strain values decreased. The higher post-annealing temperature makes it more mechanically strong, enabling the deforming forces to reduce the crystallinity and lattice deformation misalignment. The observed XRD results agreed with reported values in the literature [21-23].

The microstructural parameters of ATO films were analyzed using $\delta = [1/D^2]$, $\sigma = [E^*\langle\varepsilon\rangle]$ and $E_d = [0.5*E\langle\varepsilon\rangle^2]$ (E~200 GPa for SnO_2-Young's Modulus) [24]. Table 1 lists the structural parameters of post-annealed ATO films. Cassiterite SnO_2 has a tetragonal structure (space group: $P4_2/mnm$)and $D^{14}{}_{4h}$ symmetry. The following equations (1) and (2) were used to calculate the apical (d_1) and equatorial (d_2) distances between O and Sn.

$$d_1 = \sqrt{2}ua \quad (1)$$

$$d_2 = \sqrt{2\left(\frac{1}{2}-u\right)^2 .a^2 + \left(\frac{c}{2}\right)^2} \quad (2)$$

where a and c represent lattice constants, and u is the internal parameter which represents O^{2-} ions position at ±(0.5+u, 0.5–u, 1/2) and ± (u, u, 0) [25-27]. The basal angle (θ) is determined from the relation $\cos\theta = [a^2(1-4u+8u^2)-1] / [c^2+ 4a^2(0.5-u)^2+4a^2u^2]$ [28]. The variation in the d_1, d_2 values indicates more distorted octahedron symmetry, and the basal angle (θ) decreases with Sb^{5+}/Sn^{4+} ions. The obtained values of d_1, d_2, and θ for ATO films were tabulated in Table 2.

3.2 Surface morphological analysis

FESEM images of ATO films annealed from 150 to 350 °C are depicted in Figure 2. The film's morphology reveals a dense structure with uniformly distributed grains, smooth surfaces free of cracks, and strong substrate adhesion. The films post-annealed at 350 °C show more uniform, compact, and agglomerated [29]. The enhanced grain size was observed with thermal treatment, indicating improved crystallinity and nucleation growth rate. These results matched with XRD measurements.

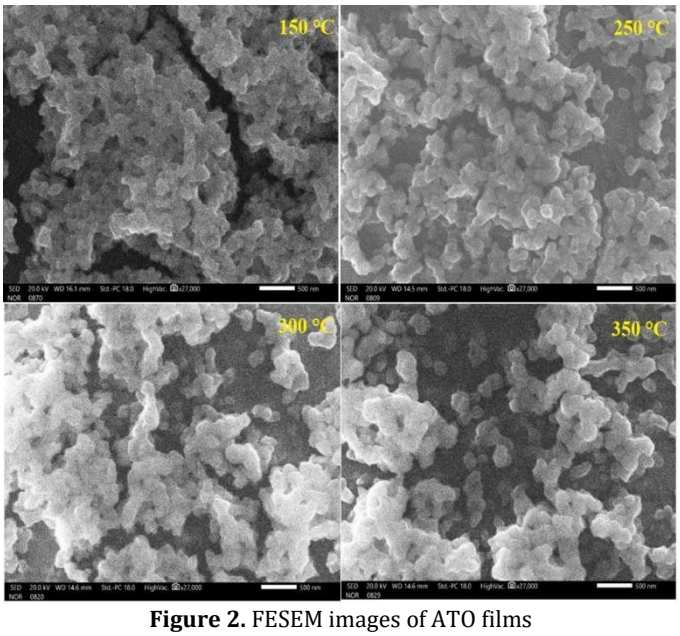

Figure 2. FESEM images of ATO films

3.3 AFM analysis

Figure 3 illustrates the morphology (2×2 μm²) of ATO films annealed from 150 to 350 °C. The grains distribute more uniformly with an increase in annealing treatment. The surface roughness parameters R_a, R_q, R_{rms}, R_{ku}, and R_{sk} were reported in Table 3. Post-annealing treatment increased Ra and R_q roughness readings from 7.20 to 14.85 nm and 8.98 to 18.63 nm. The roughness varies due to changes in grain growth kinetics during film formation [30, 31]. The increase in the roughness is due to the agglomeration of grains, which may affect the optical and electrical properties. The kurtosis (R_{ku}) and skewness (R_{sk}) roughness parameters can evaluate the surface symmetry distribution. The positive values of R_{sk} for Sb-doped SnO_2 films indicate many bumps. These roughness factors can enhance the photocatalytic capabilities of photo-detectors.

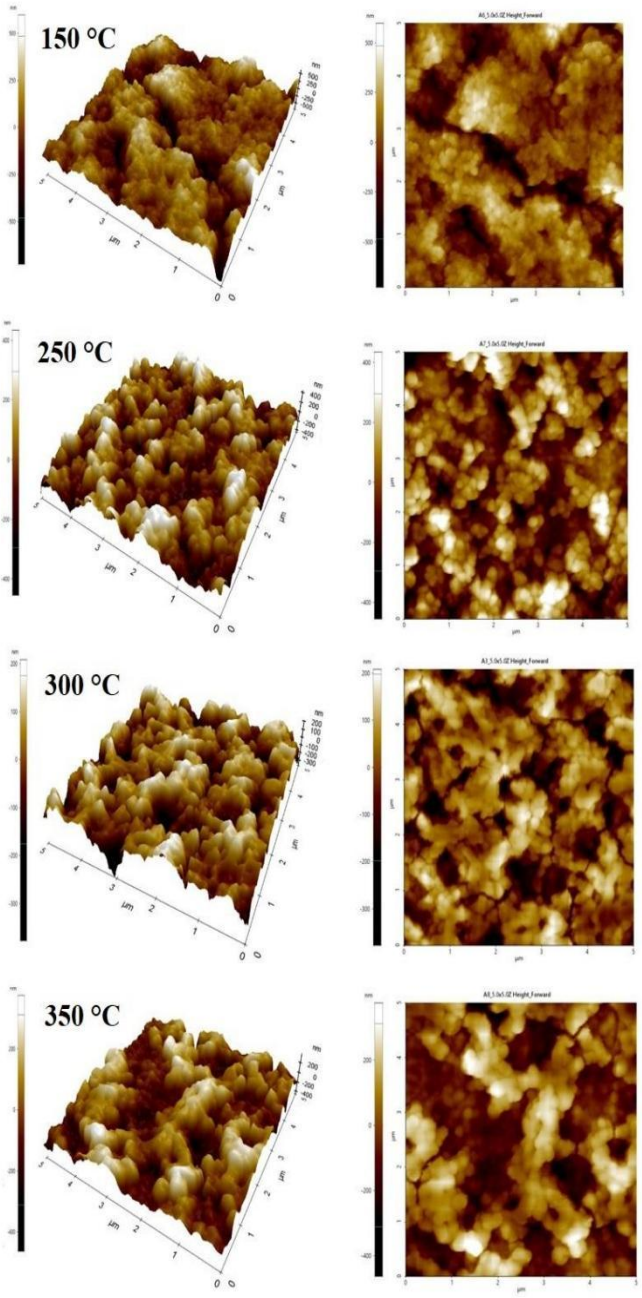

Figure 3. AFM images of ATO films

3.4 Composition analysis

The chemical valence states of ATO films were examined using XPS. The XPS complete survey spectrum for ATO film annealed at 300 °C is illustrated in Figure 4(a). XPS spectra exhibit peaks of Sn (4d), C (1s), Sn (3d), O (1s), Sn (3p), Sn (3s), and Sb (3d). Hydrocarbons may have provided the C element throughout the synthesis process. Sn $3d_{5/2}$ and Sn $3d_{3/2}$ orbitals represent the two significant peaks in the XPS spectra at 489.4 and 497.8 eV binding energies, respectively, in Figure 4(b). These two orbitals are separated by 8.4 eV, and spin-orbit splitting is assigned to Sn^{4+} ions in SnO_2 [32, 33]. Figure 4(c) demonstrates the peak corresponding to the Sb 3d core level binding. The 533.4 and 542 eV peaks belong to the trivalent states of Sb $3d_{5/2}$ and $Sb3d_{3/2}$ [34]. The XPS spectrum of O1s is exhibited in Figure 4 (d). The 532.9 eV peak corresponds to the O 1s spectrum and is assigned to the adsorbed oxygen species [35, 36].

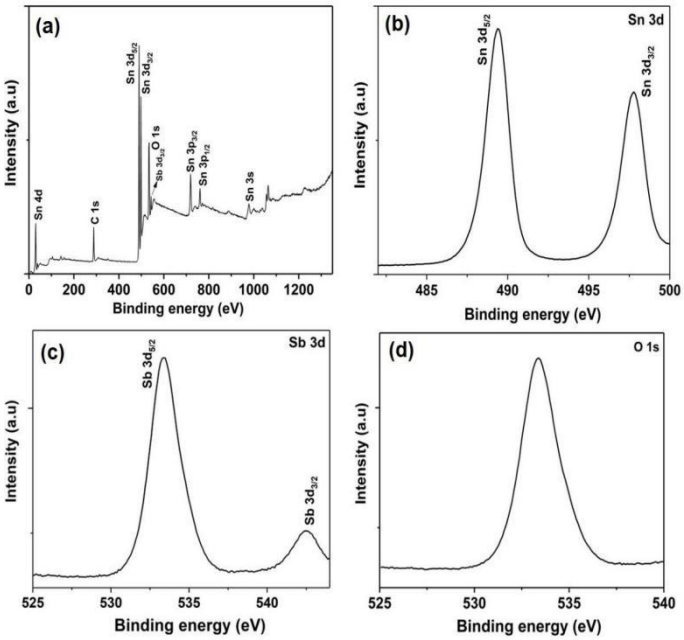

Figure 4. XPS characterization of ATO film annealed at 300 °C: a) full spectrum, b) 3d Sn , c) 3d Sb , d) 1s O spectra

3.5 Optical studies

Figure 5(a) shows the optical absorption spectra of ATO films post-annealed from 150 to 350 °C. The absorption edge of the films exhibits a red shift, leading to a reduction in carrier confinement due to enhanced crystallite size. Tauc's equation relates the absorption coefficient and photon energy as

$$\alpha h\nu = A\left(h\nu - E_g\right)^{1/2} \quad (3)$$

The extrapolation from the curve $(\alpha h\nu)^2$ versus hν of ATO films is shown in Figure 5b. The band gap reduced from 3.36 to 3.08 eV by increasing post-annealing temperature from 150 to 350 °C. The red shift in the optical band gap is due to reduced defect densities and grain boundaries [37, 38]. The

Burstein-Moss effect describes a variation of E_g with 'n' and is given by the relation. [39]

$$\Delta E_g^{BM} = \frac{h^2}{8m_e^*}\left(\frac{3}{\pi}\right)^{2/3} n^{2/3} \quad (4)$$

where h, m^*_e, and n represent Planck's constant, the effective mass of the electron, and carrier concentration. The carrier concentration of ATO films is significantly affected by post-annealing temperature. Increased Sb^{5+} ions increased carrier concentration from 3.43×10^{21} to 3.91×10^{21} cm^{-3}, as they added two electrons. The same behavior trend in increasing carrier concentration has been discovered in other research works [40, 41].

The electronegativity concept is utilized for estimating the edge potentials of the conduction band (E_{VB}) as well as the valence band (E_{VB}) of ATO thin films with [42]

$$E_{VB} = \chi - E_e + 0.5E_g \quad (5)$$

$$E_{CB} = E_{VB} - E_g \quad (6)$$

where χ (for SnO_2~6.24 eV) represents electronegativity. E_e refers to the free electron energy ~4.5 eV. The E_{VB} values for ATO thin films annealed at 150, 250, 300, and 350 °C were obtained as 3.42, 3.39, 3.34, and 3.28. The related E_{CB} values are 0.06, 0.09, 0.14, and 0.20 eV.

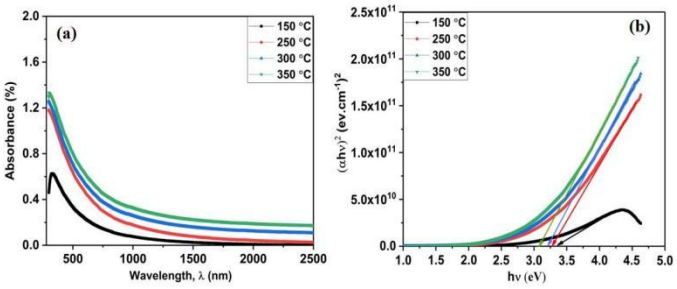

Figure 5. Plots of (a) Optical absorption spectra and (b) $(\alpha h\nu)^2$ versus hν for ATO films

The variation of refractive index (n) with wavelength for ATO films annealed from 150 to 350 °C was illustrated in Figure 6(a). The refractive index shows normal dispersion behavior with the wavelength. It may be due to the reduced absorption coefficient with wavelength. The increase in 'n' with annealing treatment proves the $E_g n^4$ ~ constant given by the Moss relation [43]. Refractive index enhancement accompanies decreases in the band gap value. The 'n' of ATO films was estimated from the relation Moss [44, 45]

$$E_g n^4 = k \quad (7)$$

where k =108 eV. The relation between E_g and n given by Herve and Vandamme (HV) [46, 47] as

$$n = \sqrt{1 + \left(\frac{A}{E_g + B}\right)^2} \quad (8)$$

where A=13.6 and B=3.4 eV are constant at 13.6 and 3.4 eV, respectively. Figure 6(b) depicts the refractive index computed based on the above relations at various post-annealing temperatures. The 'n' value increased from 2.38 to 2.43 (Moss relation) and from 2.24 to 2.32 (HV relation). The variation in 'n' values with post-annealing temperature indicates improved crystallinity and decreased defects. The increase in the refractive index values could also be attributed to a decrease in carrier concentration and grain size enhancement [48]. The dielectric properties of the materials, such as static and high-frequency constants, were critical for electro-optical devices.

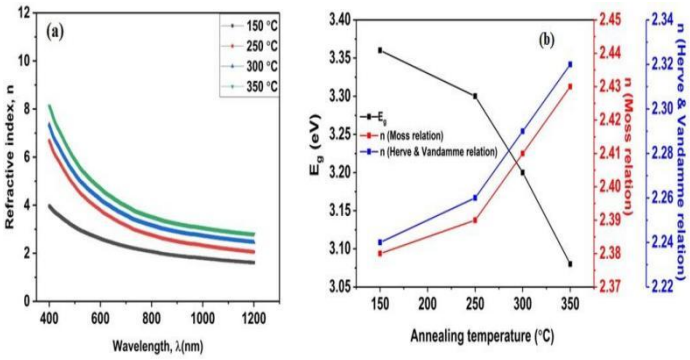

Figure 6. Variation of (a) n vs λ and (b) E_g with post-annealing temperature for ATO films

The high-frequency and static dielectric constant (ε_∞ and ε_o) of ATO films were estimated from the equations [49]

$$\varepsilon_\infty = n^2 \quad (9)$$

$$\varepsilon_o = 18.52 - 3.08\,E_g \quad (10)$$

Table 4 reports the higher ε_∞ and ε_o values due to atom composition and structure changes. The post-annealing temperature improves the optical properties of ATO films compared to previously reported results [50,51].

3.6 Electrical properties

Figure 7 illustrates ATO films n, μ, and ρ with varying post-annealing temperatures. The electrical resistivity (ρ) of ATO films decreased from 2.64×10^{-3} to 1.74×10^{-3} Ω.cm. The reduced electrical resistivity is due to the substitutional doping of Sb and the decreased interstitial atoms. The carrier concentration(n) depends on the dopant charge state and concentration. The carrier mobility(μ) varies with the surface defects, oxygen stoichiometry, structural defects, etc. [52]. The sheet resistance values for ATO thin films were evaluated using the formula, $R_s = \rho/t$. The R_s values of ATO films annealed at 150, 250, 300, and 350°C were obtained as 94.3, 80.4, 68.6, and 62.1 Ω/sq. The decreased sheet resistance with increased post-annealing temperature is due to improved free carrier concentration. This behaviour is because of Sb^{5+} substitution by Sn^{4+} ions in the SnO_2 lattice, which introduces the charge carriers by generating excess electrons. The post-annealing effect enhanced the ATO film's electrical properties compared to previously reported values [53, 54].

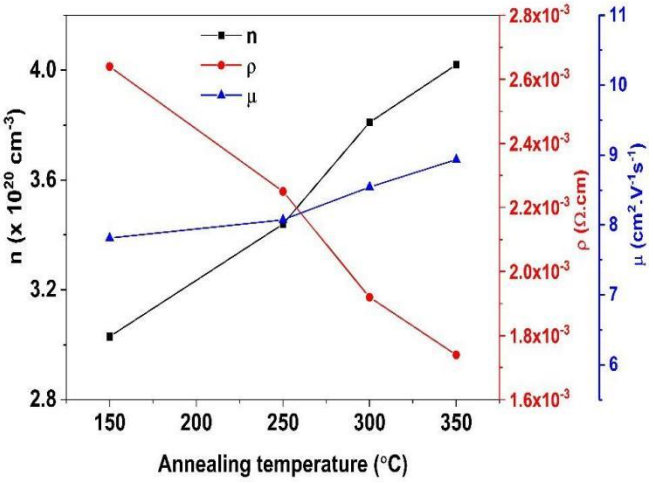

Figure 7. Plot of n, ρ, and μ of ATO films

Table 1. Structural parameters of ATO films

Structural parameters	Annealing temperature (°C)			
	150	**250**	**300**	**350**
FWHM,β (°)	4.32	3.55	2.82	2.28
d-value (nm)	0.3305	0.3374	0.3404	0.3411
Lattice constant, a (Å)	0.4673	0.4771	0.4813	0.4824
Lattice constant, c (Å)	0.3188	0.3224	0.3258	0.3326
Volume, V =a^2c $(Å)^3$	69.6	73.41	75.48	77.4
Crystallite size, D (nm)	19	23	32	45
Micro strain, ε ($line^{-2}.m^{-4}$)	0.018	0.015	0.012	0.0096
Dislocation density, δ, $\times10^{15}$ (nm^{-2})	2.77	1.89	0.97	0.45
Stress, σ (GPa)	3.664	3.014	2.395	1.937
Energy density, $E_d \times10^6$ ($J.m^{-3}$)	33.56	22.72	14.34	9.38

Table 2. Apical and equatorial (d_1 and d_2) distances, internal parameter (u), and basal angle (θ) of ATO films

Annealing temperature (°C)	**u**	**d_1 (Å)**	**d_2(Å)**	**θ (˚)**
150	0.341	2.254	1.908	24.42
250	0.338	2.280	1.948	23.99
300	0.334	2.303	1.965	23.76
350	0.344	2.352	1.972	23.56

Table 3. Surface roughness parameters of ATO films

Annealing temperature (°C)	**R_q (nm)**	**R_a (nm)**	**R_{ku}**	**R_{sk}**
150	8.98	7.20	0.063	2.86
250	11.46	10.83	0.090	2.68
300	13.38	11.67	0.548	2.33
350	18.63	14.06	0.385	3.29

Table 4. E_g, n, ε_∞, and ε_o values for ATO films

Annealing temperature (°C)	E_g (eV)	Moss relation		Herve & Vandamme		ε_o
		n	ε_∞	n	ε_∞	
150	3.36	2.38	5.67	2.24	5.04	8.17
250	3.30	2.39	5.72	2.26	5.12	8.35
300	3.20	2.41	5.80	2.29	5.24	8.66
350	3.08	2.43	5.92	2.32	5.40	9.03

4. CONCLUSIONS

ATO films were grown by sol-gel spin coating and post-annealed in the 150-350 °C range. XRD patterns of ATO films exhibit a rutile tetragonal structure. The FWHM values of the peaks decreased from 4.32 to 2.28°, and the intensities of the diffraction peaks increased with post-annealing treatment, indicating improved crystallinity and defect minimization. The surface morphology of ATO films exhibits higher surface roughness with post-annealing treatment. The absorption edge moves towards higher wavelengths, reducing the band gap from 3.36 to 3.08 eV. The thermal annealing treatment expands the crystal lattice, weakens the interatomic bonds, and reduces the bandgap. The reduction in the ATO film's electrical resistivity and sheet resistance can be due to increased oxygen (O) vacancies, which facilitate charge carrier concentration. The results obtained for thermally annealed ATO films indicate they might be a viable electrode for optoelectronic device applications.

ACKNOWLEDGMENTS

The facilities (FESEM, AFM, and XPS) available at CeNSE, IISc, Bengaluru were used to perform this research work.

REFERENCES

[1] Wenhao Yang, Shihui Yu, Yang Zhang, and Weifeng Zhang, "Properties of Sb-doped SnO_2 transparent conductive thin films deposited by radio-frequency magnetron sputtering," *Thin solid films*, vol. 542, pp. 285-288, 2013.

[2] Abhijit A. Yadav, S.C. Pawar, D.H. Patil, and M.D. Ghogare, "Properties of (200) oriented, highly conductive Sno_2 thin films by chemical spray pyrolysis from non-aqueous medium: effect of antimony doping," *Journal of Alloys and Compounds,* vol. 652, pp. 145- 152, 2015.

[3] Laxmikanta Dua and Prasanta K. Biswas, "Synthesis and photoluminescence property of nanostructured sol–gel antimony tin oxide film on silica glass," *Chemical Physics Letters,* vol.572, pp. 66 – 72, 2013.

[4] H. Xiong, B.L. Zhu, J.Q. Zhang, J. Wu, X.W. Shi, and W.Q. Sun," Combined effects of substrate temperature and post annealing temperature on structural, optical and electrical properties of Sb-doped SnO_2 films," *Journal of Alloys and Compounds,* vol. 997, pp.174970 , 2024.

[5] V.N. Zhitomirsky, T. David, R.L. Boxman, S. Goldsmith, A. Verdyan, Ya. M. Soifer, and L. Rapoport, "Properties of SnO_2 coatings fabricated on polymer substrates using filtered vaccum arc deposition," *Thin Solid Films,* vol. 492, no 1- 2, pp. 187 – 194, 2005.

[6] A.R. Babar, S.S. Shinde, A.V. Moholkar, C.H. Bhosale, J.H. Kim, and K.Y. Rajpure, "Physical properties of sprayed antimony doped tin oxide thin films: The role of thickness," *Journal of Semiconductors*, vol. 32, no.5, pp. 053001 , 2011.

[7] Khaoula Derrar, Mourad Zaabat, Nouhad Rouabah, Roshan Nazir, Faouzi Hanini, Abdelkader Hafdallah, Sher Afghan Khan, Norah Salem Alsaiari, Khadijah Mohammedsaleh Katubi, and Khamael M. Abualnaja, "Preparation of Sb;SnO_2 thin films and its effect on opto-electrical properties," *Journal of Materials Science: Materials in Electronics,"* vol. 33, pp. 10142 – 10153, 2022.

[8] Steven B.O. dos Santos, Joao V.M. Lima, Miguel H. Boratto, and Luis V.A. "Influence of substrate temperature on the deposition of the homostructure SnO_2:Sb/SnO_2:Er via sol-gel dip-coating," *Ferroelectrics*, vol. 545, no. 1, pp. 10–21, 2019.

[9] R. F. Martinez-Gazoni, M. W. Allen, and R. J. Reeves, "Conductivity and transparency limits of Sb-doped SnO_2 grown by molecular beam epitaxy," *Physical Review B,* vol.98, pp. 155308, 2018.

[10] Junji Sawahata and Tasuku Kawasaki, "Structural and electrical properties of Sb-doped SnO_2 thin films prepared by metal organic decomposition," *Thin Solid Films*, vol. 685, pp. 210 – 215, 2019.

[11] Jonty I. Scott, Rodrigo F. Martinez-Gazoni, Martin W. Allen, and Roger J. Reeves, "Optical and electronic properties of high-quality Sb-doped SnO_2 thin films grown by mist chemical vapour deposition," *Journal of Applied Physics,* vol.126, pp. 135702/1 -9, 2019.

[12] Hai-Ying Du, Jing Wang, Peng Yu, Nai-Seng Yu, Yan-Hui Sun, and Jiang-Li Tian, "Investigation of gas sensing materials tin oxide nanofibers treated by oxygen plasma," *Journal of Nanoparticle Research,* vol.16, pp. 2216/1 – 10, 2014.

[13] A.R. Babar, S.S. Shinde, A.V. Moholkar, C.H. Bhosale, J.H. Kim, and K.Y. Rajpure, "Sensing properties of sprayed antimony doped tin oxide thin films: Solution molarity," *Journal of Alloys*

and Compounds, vol.509, no. 6, pp. 3108 – 3115, 2011.

[14] N. M. Shaalan, M. Rashad, and T. Yamazaki, "Sensing performance of SnO_2 film fabricated by sputtering deposition," *Applied Physics A,* vol. 120, no.4, pp. 1555 – 1563, 2015.

[15] S. Jäger, B. Szyszka, J. Szczyrbowski, and G. Bräuer, "Comparison of transparent conductive oxide thin films prepared by a.c. and d.c, reactive magnetron sputtering," *Surface and Coating Technology,* vol.98, no. 1- 3, pp. 1304 – 1314, 1998.

[16] H. Kim and A. Piqué, Transparent conducting Sb-doped SnO_2 thin films grown by pulsed-laser deposition," *Applied Physics Letters,* vol.84, pp. 218 – 220, 2004.

[17] B. Thangajaru, "Structural and electrical studies on highly conducting spray deposited fluorine and antimony doped SnO_2 thin films from $SnCl_2$ precursor," *Thin Solid Films*, vol. 402, pp. 71-78, 2002.

[18] C. Terrier, J.P. Chatelon, and J.A. Roger, "Electrical and optical properties of Sb:SnO_2 thin films obtained by the sol-gel method," *Thin Solid Films* vol. 295, no. 1- 2, pp. 95-100, 1997.

[19] R. Ramarajan, M. Kovendhan, K. Thangaraju, D. Paul Joseph, R. Ramesh Babu, and Viswanathan Elumalai, "Enhanced optical transparency and electrical conductivity of Ba and Sb co-doped SnO_2 thin films," *Journal of Alloys and Compounds,* vol. 823, pp. 15370/1 – 11, 2020

[20] B.Benrabah, A. Bouaza, S.Hamzaoui, and A.dehbi, Sol-gel preparation and characterization of antimony doped tin oxide (ATO) powders and thin films," *The European Physical Journal Applied Physics,"* vol. 48, no. 3, pp. 30301 / 1 – 5, 2009.

[21] M.K. Hussen and F.B. Dejene, "Influence of annealing temperature on material properties of red emitting $ZnGa_2O_4$: Cr^{3+} nanostructures," *Journal of Sol-Gel Science and Technology,* vol. 88, pp. 454 – 464, 2018.

[22] Jiann-Shing Jeng, "The influence of annealing atmosphere on the material properties of sol-gel derived SnO_2:Sb films before and after annealing," *Applied Surface Science*, vol. 258, no. 16, pp. 5981 – 5986, 2012.

[23] G. Gasparro, J. Pütz, D. Ganz, and M.A. Aegerter, "Parameters affecting the electrical conductivity of SnO_2:Sb sol-gel coatings," *Solar Energy Materials and Solar Cells,* vol. 54, no. 1 – 4, pp. 287- 296, 1998.

[24] Ahmad A. Ahmad, A.B. Migdadi, and Qais M. Al-Bataineh, "Structural, optical, and electrical properties of strontium-doped tin dioxide films for higher photoconductivity," *Thin Solid Films*, vol.796, pp. 140312/ 1 – 7, 2024.

[25] D.Subramanyam, B. Rajesh Kumar, and K. Chandrasekhar Reddy, "Micro-Structural, Surface Morphological, and Optical Properties of Sol–Gel Spin Coated Sb-Doped SnO_2 Thin Films," *Physics of the Solid State*, vol. 67, no. 1, pp. 17–26, 2025.

[26] Aashish Kumar, Naveen Kumar, Mansi Chitkara, and Gulshan Dhillon, "Physicochemical investigations of structurally enriched Sm^{3+} substituted SnO_2 nano crystals," *Journal of Materials Science: Materials in Electronics,* vol. 33, pp. 5283- 5296, 2022.

[27] Soumen Das and V. Jayaraman, SnO_2: A comprehensive review on structures and gas sensors," *Progress in Materials Science,* vol. 66, pp. 112 – 255, 2014.

[28] F.H Aragon, J.A.H. Coaquira, L. Villegas-Lelovsky, S. W da Silva, D. F. Cesar, L. C. C. M. Nagamine, R. Cohen, E. Menendez-Proupin, and P.C Morais, "Evolution of the doping regimes in the Al-doped SnO_2 nanoparticles prepared by a polymer precursor method," *Journal of Physics: Condensed Matter,* vol. 27, pp. 095301/1–8, 2015.

[29] Davender Singh, Virender Singh Kundu, and A.S. Maan, "Structural, morphological and gas sensing study of zinc doped tin oxide nano particles synthesized via hydrothermal technique," *Journal of Molecular Structure,* vol. 1115, pp. 250 – 257, 2016.

[30] R. Ramarajan, M. Kovendhan, K. Thangaraju, and D. Paul Joseph, "Substrate Temperature Dependent Physical Properties od Spray Deposited Antimony-Doped SnO_2 Thin Films," *Thin Solid Films*, vol. 704, pp. 137988/1–10, 2020.

[31] J. Mazlooma, F.E. Ghodsia, and M. Gholami, "Fiber-like stripe ATO (SnO_2:Sb) nanostructured thin films grown by sol-gel method: Optical, topographical and electrical properties" *Journal of Alloys and Compounds,* vol. 579, pp. 384-393,2013.

[32] Liwei Wang, Jintao Li, Yinghui Wang, Kefu Yu, Xingying Tang, Yuanyuan Zhang, and Shaopeng Wang Chaoshuai Wei, "Construction of 1D SnO_2-coated ZnO nanowires heterojunction for their improved n-butylamine sensing performances", *Scientific Reports,* vol .6, no.1, 35079/1 – 12, 2016.

[33] Meihua Li, Chao Mou, Yunfan Zhang, Xiao Li, Huichao Zhu, and Guangfen Wei, "Zn-doped SnO_2 nanoparticles for ethanol vapour sensor: a combined experimental and first-principles study," *Journal of Materials Science: Materials in Electronics,* vol.34, no. 12, pp. 1059/ 2023.

[34] Yanfen Niu, Libing Duan, Xiaoru Zhao, Cong Han, Jiale Guo, Wangchang Geng, "Effect of Sb doping on structural and photoelectric properties of SnO_2 thin films" *Journal of Materials Science: Materials in Electronics,* vol. 31, pp. 3289/1 – 14, 2020.

[35] Jyh Ming Wu, "A room temperature ethanol sensor made from p-type Sb-doped SnO_2 nanowires," *Nanotechnology,* vol. 21, no.23, pp.235501/1 -7, 2010.

[36] A.R. Babar, S.S. Shinde, A.V. Moholkar, C.H. Bhosale, J.H. Kim, and K.Y. Rajpure, "Structural and optoelectronic properties of antimony incorporated tin oxide thin films," *Journal of Alloys and Compounds,* vol.505, no.2, pp. 416 – 422, 2010.

[37] J. Ungula, B.F. Dejene, and H.C. Swart, "Effect of annealing on the structural, morphological and optical properties of Ga-doped ZnO nanoparticles by reflux precipitation method," *Results in Physics,* vol. 7, pp.2022 – 2027, 2017.

[38] A. Sadeghzadeh-Attar and M.R. Bafandeh, "The effect of annealing temperature on the structure and optical properties of well-aligned 1D SnO_2 nanowires synthesized using template-assisted deposition,"*Crystal Engineering Communications*, vol.20**,** no.4, pp. 460-469, 2018.

[39] J.G. Lu, S. Fujita, T. Kawaharamura, H. Nishinaka, Y. Kamada, T.Ohshima, Z.Z. Ye, Y. J. Zeng, Y. Z. Zhang, L. P. Zhu, H. P. He, and B. H. Zhao, "Carrier concentration dependence of band gap shift in n-type ZnO:Al film," *Journal of Applied Physics,* vol.101, no.8, pp. 083705/1 – 8, 2007.

[40] E.Elangovan, S.A. Shivashankar, and K. Ramamurthi, "Studies on structural and electrical properties of sprayed SnO_2:Sb films," *Journal of Crystal Growth,* vol.276, no.1 – 2, pp. 215 -221, 2005.

[41] E. Elangovan, K. Ramesh, and K. Ramamurthi, "Studies on structural and electrical properties of spray deposited SnO_2:Sb thin films as a function of substrate temperature,"*Solid State Communications,* vol.130, no.8, pp. 523-527, 2004.

[42] J. Wang, C. Lu, X. Liu, Y. Wang, Z. Zhu, and D. Meng, Synthesis of tin oxide (SnO & SnO_2) micro/ nanostructures with novel distribution characteristic and superior photocatalytic performance," *Materials and Design,* vol. 115, pp. 103 – 111, 2017.

[43] M. Ali Yıldırım, Sümeyra Tuna Yıldırım, Emine Fedakar Sakar, and Aytunç Ates, "Synthesis, characterization and dielectric properties of SnO_2 thin films," *Spectrochimica Acta Part A: Molecular and Biomolecular Spectroscopy,* vol. 133, 60 – 65, 2014.

[44] M.A. Yıldırım, "The effect of copper concentration on structural, optical and dielectric properties of $Cu_xZn_{1-x}S$ thin films," *Optics Communications,* vol.285, no. 6, pp.1215 - 1220 2012.

[45] L. Hannachi and N. Bouarissa, "Band parameters for cadmium and zinc chalcogenide compounds," *Physica B: Condensed Matter*, vol.404, no. 20, pp. 3650-3654, 2009.

[46] F. Mezrag, W.K. Mohamed, and N. Bouarissa, "The effect of zinc concentration upon optical and dielectric properties of $Cd_{1-x}Zn_xSe$," *Physica B: Condensed Matter*, vol. 405, no.9, pp. 2272-2276, 2010.

[47] P. Herve, and L.K.J. Vandamme, "General relation between refractive index and energy gap in semiconductors," *Infrared Physics & Technology,* vol.35, no.4, pp. 609 – 615, 1994.

[48] S.W. Xue, X.T. Zu, W.G. Zheng, H.X. Deng, and X. Xiang, "Effects of Al doping concentration on optical parameters of ZnO:Al thin films by sol-gel technique," *Physica B: Condensed Matter*. vol. 381, no.1- 2, pp. 209- 213, 2006.

[49] S. Adachi, "Properties of Group IV, III–V and II–VI Semiconductors," *John Wiley & Sons, Ltd,* 2005.

[50] S.H. Mohamed, N.M.A. Hadia, M.F. Hasaneen, and M.A. Hassan, "Morphologies and optical properties of mixed tin oxysulfide produced by evaporation condensation of SnS," *Materials Science in Semiconductor Processing,* vol. 72, pp. 72 – 77, 2017.

[51] Ali A. Yousif,Reeman M. Hathal, and Husam R. Abed, "The Effectiveness of Decorating Antimony on the Structural, Optical, and Electrical Characteristics of SnO_2 Nanowires," *Journal of Electronic Materials,* vol.50, pp. 5442 – 5452 , 2021.

[52] B. Salameh and A.M. Alsmadi, "Enhanced optoelectronic properties of spray deposited antimony-doped tin oxide thin films," *Surfaces and Interfaces,* vol.55, pp. 105327, 2024.

[53] J.W. Leem and J.S. Yu, "Physical properties of electrically conductive Sb-doped SnO_2 transparent electrodes by thermal annealing dependent structural changes for photovoltaic applications," *Materials Science and Engineering: B,* vol.176, no. 15, pp. 1207 – 1212, 2011.

[54] S.U. Lee, B. Hong, and J.H. Boo, "The Effect of Annealing Atmospheres on Structural, Electrical and Optical Properties of the ATO films prepared by RF Magnetron Sputtering," *Functional Materials Letters,* vol.3, no.2, pp. 119 – 123, 2010.